

DIGITAL ELEVATION MODELS OF THE LUNAR SURFACE. A. C. Cook¹ and M. S. Robinson², ¹Center for Earth and Planetary Studies, National Air and Space Museum, Washington DC 20560-0315, USA (tcook@ceps.nasa.gov), ²Department of Geological Sciences, Northwestern University, Evanston IL 60208-2150, USA (robinson@eros.earth.nwu.edu).

Introduction: Several Digital Elevation Models (DEMs) have been produced at a scale of 1km/pixel and covering ~1/5th of the lunar surface. These were produced mostly by semi-automatically matching the stereo available between Clementine UVVIS images, although some localized DEMs have been produced by applying this technique to Apollo Metric stereo pairs, or by digitizing an existing Apollo Metric contour map. The DEMs that result from Clementine UVVIS images, although of poorer height accuracy (± 300 - 600 m for a single matched point) [1] than the Clementine laser altimeter point measurements ($< \pm 100$ m) [2], do provide considerably higher spatial resolution (e.g. every kilometer versus every tens of kilometers) and allow topography in the polar regions to be determined.

Method: Nadir pointing Clementine UVVIS stereo pairs are automatically stereo matched using a patch-based matcher [3] and fed through a stereo intersection camera model to yield a digital terrain model (DTM) of longitude, latitude, height points. The DTM for each stereo pair is then re-plotted and interpolated to form map-projected DEM tiles. The DEM tiles can then be fitted to absolute height laser altimeter points, or iteratively to each other, to form a DEM mosaic. Uncertainties in UVVIS camera pointing and the need to accumulate a sufficiently good topographic S/N ratio necessitates the use of 1km pixels for the UVVIS derived DEMs. For Apollo Metric stereo, an internal camera geometry correction and a full photogrammetric block adjustment must be performed using ground control points to derive a DEM. The image scale of Apollo Metric, and the stereo angle, allow for a DEM with 100m pixels, and a height accuracy of ± 25 m. Apollo Metric imagery had previously been used to derive contour maps for much of the lunar equatorial regions, however to recover this information in digital form these maps must be digitized.

Regions covered: Most of the mare areas mapped contain noticeable topographic noise (see figure 1). This results from the stereo matcher failing in regions of low texture and contrast. Below is a summary of the regions for which DEMs have been generated, and some of the features visible in each (heights are referenced to a 1738km radius sphere):

Apollo 15 landing site ($1^{\circ}E$ - $7^{\circ}E$, $20^{\circ}N$ - $30^{\circ}N$). Features include Hadley rille (just visible) and several mountains [4].

Apollo 17 landing site ($30.0^{\circ}E$ - $31.5^{\circ}E$, $19.5^{\circ}N$ - $21.0^{\circ}N$). This DEM was derived by digitizing con-

tours from a map [5].

Alpine Valley ($2^{\circ}W$ - $8^{\circ}E$, $47^{\circ}N$ - $51^{\circ}N$). The valley and Trouvelot crater are visible [6]. Topography ranges from +1km to -4km. The valley walls are <1km high.

Aristarchus ($60^{\circ}W$ - $40^{\circ}W$, $20^{\circ}N$ - $30^{\circ}N$). Features visible include Aristarchus craters, Vallis Schröteri, and the craters: Herodotus, Schiaparelli, and Prinz.

Copernicus crater ($30^{\circ}W$ - $10^{\circ}W$, $0^{\circ}N$ - $20^{\circ}N$). Features visible include Montes Carpatum and the craters: Copernicus, Eratosthenes, Reinhold, and Tobias Mayer.

Giordano Bruno crater ($101^{\circ}E$ - $106^{\circ}E$, $33^{\circ}N$ - $38^{\circ}N$). This DEM [7] reveals approximately 60% of the crater interior.

Kepler crater ($38^{\circ}W$, $8^{\circ}N$). Using this DEM [7] a perspective view of this crater have been produced with a USGS color-ratio map overlaid.

Korolev Basin ($175^{\circ}W$ - $160^{\circ}W$, $10^{\circ}S$ - $20^{\circ}N$). 75% of the Korolev basin is present in this DEM together with a pre-Nectarian basin the size of Korolev just to the north [8]. The topography in this DEM ranges from 0km to +9.6km. Named craters visible include Mach, McMath, Icarus, and Tsander.

Luna 9/13 landing site ($70^{\circ}W$ - $60^{\circ}W$, $0^{\circ}N$ - $30^{\circ}N$). The topographic range is from ~0km to -4.5km, the latter being on the floor of Hevelius A crater.

Mare Crisium ($50^{\circ}E$ - $70^{\circ}E$, $0^{\circ}N$ - $20^{\circ}N$). This DEM [4] covers the lower half of the basin and surrounding highlands. The topographic range is from +3km to -5km. Several protruding floor crater rims are visible on the basin floor e.g. Picard, Yerkes, and Lick.

Mare Orientale ($120^{\circ}W$ - $75^{\circ}W$, $40^{\circ}S$ - $0^{\circ}N$). This area was covered well in stereo, and a regional north-south slope is detectable across the basin [9]. The topography varies from +6km on the western rim to -5km on the bottom of Maander crater. Three rings of the basin are clearly visible in the topography.

Mare Serenitatis ($10^{\circ}E$ - $40^{\circ}E$, $10^{\circ}N$ - $40^{\circ}N$). Highland areas are well depicted in the DEM and so are the craters include Bessel, Dawes, Le Monier, Mene-laus, Plinius, Posidonius, and Ross.

North polar region (60° - 90°). An analysis of this DEM [10,11] revealed the newly discovered Sylvester-Nansen pre-Nectarian impact basin (300-400km diameter, centered on $45^{\circ}E$, $83^{\circ}N$). The Schwarzschild and Be'lkovich basins are clearly visible as well as the northern extent of the Imbrium basin. Several secondary ejecta scour marks are present in the topography and spread out radially from Mare Imbrium. The crater

Hayn contains a north-south running graben which bisects its central peaks.

Saha crater area (90°E-105°E, 5°S-5°N). Stereo imagery is missing in the center of this region [7].

Schickard (60°W-50°W, 50°S-40°S). The floor interior craterlets and surrounding highlands are clearly visible[7].

Sinus Iridum (40°W-30°W, 30°N-50°N). See figure 1 [4].

South polar region (90°S-60°S). An analysis of this DEM [4,7,10-15] has revealed two newly discovered pre-Nectarian impact basins (Schrodinger-Zeeman, 250km in diameter, centered on 165°W, 81°S, and 330km diameter Bailly-Newton, centered on 57°W, 73°S). Several other prominent basins are visible including the southern half of the South Pole-Aitken (SPA) basin, Bailly, Schrodinger, part of Clavius, and the Amundsen-Ganswindt basin. The topographic range in this DEM is considerably greater than the north polar DEM due to the presence of the SPA topography.

Tsiolkovsky (124°E, 19°S). In this DEM [16] the western flanks of Tsiolkovsky are shown in great detail.

Tycho (20°W-0°W, 50°S-40°S). This DEM shows Tycho crater and its surrounds and the northern interior of Maginus crater

Discussion: The best results obtained from stereo matching lie over highland regions where there exists much surface texture for the stereo matcher to lock onto. Mare regions are darker and relatively featureless and hence result in noisy DEMs which largely preclude the detection of wrinkle-ridges. Nevertheless craters and peaks within mare areas can be resolved and profiles extracted from these features. One of the drawbacks of the Clementine derived DEMs is that the stereo coverage at latitudes below $\pm 60^\circ$ in latitude contain many gaps. However when compared to an interpolated Clementine laser altimeter DEM [2], the stereo derived DEM contains considerably more spatial detail. The DEMs produced from Clementine stereo are also complementary to Clementine laser altimeter measurements, because the latter perform better over flat mare areas, but less well in highland regions. Some of these DEMs are available on the following web address:

<http://www.nasm.edu/ceps/research/cook/topo.html>

References: [1] Cook A.C. et al (1997) *Planet. Space. Sci.*, 44, 1135–1148. [2] Smith D.E. et al (1997) *JGR*, 102, 1591–1611. [3] Day T. et al (1992) *Int. Arch. Photogr. Remot. Sens.*, 29-B4, 801–808. [4] Cook A. C. et al (1996) Proc. 24th Vernadsky-Brown micro., Moscow. [5] Robinson et al (1999) LPI XXX, Abstract #1931. [6] Cook A. C. and Hiesinger H. (1996) *LPS XXVII*, 249–250. [7] Cook A. C. et al. (1996) *An. Geophys.* 14(III), C803. [8] Konopliv A.

(1999) private communication. [9] Cook A. C. et al. (1997) *An. Geophys.*, 15(III). [10] Cook A. C. et al. (1999) *LPS XXX*, Abstract #1154. [11] Cook A. C. et al. (1999) *JGR*, submitted. [12] Hoffmann H. et al. (1996) *An. Geophys* 14(III). [13] Cook A. C. and Robinson M. S. (1998) *3rd Int. Conf. Expl. and Utiliz. of the Moon*, Moscow, 21. [14] Spudis P. D. et al. (1998) *Proc. of New Views of the Moon I*. [15] Cook A. C. and Robinson M. S. (1998) *3rd Int. Conf. Expl. and Utiliz. of the Moon*, Moscow, 21. [16] Cook A. C. et al. (1994) *Bull. Amer. Astron. Soc.*, 26, 1097.

Acknowledgments: We would like to thank DLR Berlin for the computing time available for some of the earlier DEMs, and University College London/Laser-Scan for the Gotcha stereo matching software, originally written by Tim Day.

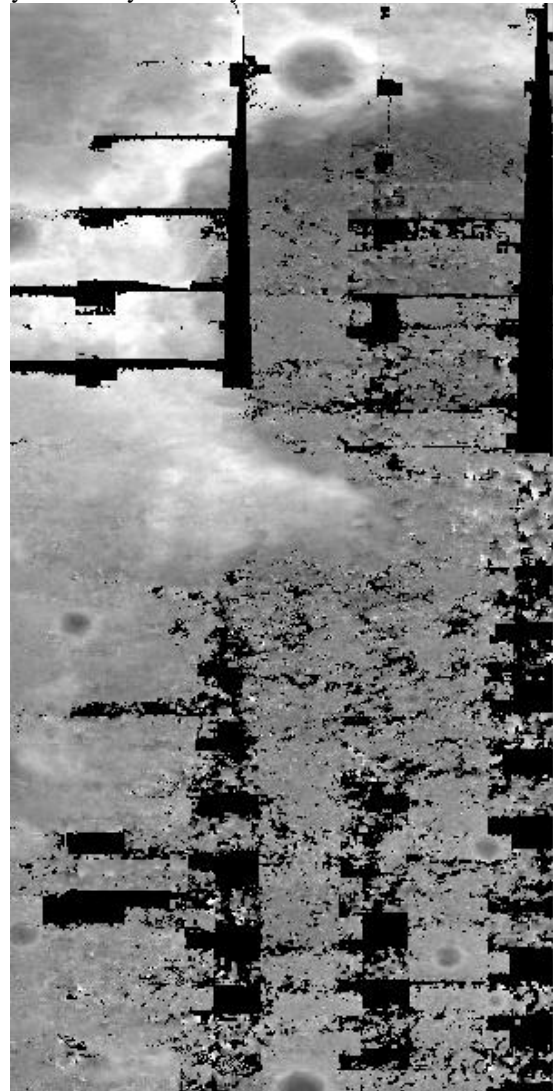


Fig. 1. DEM of Sinus Iridum. Black=low (or no data) and white=high.